

Two-dimensional Navier–Stokes simulation of breaking waves

Gang Chen and Christian Kharif

*Institut de Recherche sur les Phénomènes Hors Equilibre, UMR CNRS 138, Case 903,
163, avenue de Luminy, 13288 Marseille Cedex 9, France*

Stéphane Zaleski and Jie Li

*Laboratoire de Modélisation en Mécanique, URA CNRS 229, Université Pierre et Marie Curie,
4 place Jussieu, 75252 Paris Cedex 05, France*

Abstract

Numerical simulations describing plunging breakers including the splash-up phenomenon are presented. The motion is governed by the classical, incompressible, two-dimensional Navier-Stokes equation. The numerical modelling of this two-phase flow is based on a piecewise linear version of the volume of fluid method. Capillary effects are taken into account as a stress tensor computed from gradients of the volume fraction function. Preliminary results concerning the time evolution of liquid–gas interface and vorticity field are given for short waves, showing how an initial steep wave undergoes breaking and successive splash-up cycles. Different evolutions of the wave energy are observed during the breaking stage. The energy dissipation due to viscosity becomes significantly important at each time of the impact of jet and the formation of splash-up. It is found that nearly 70% of the wave energy is lost after about three periods.

Plunging breakers are due to the formation of a jet at the crest of the wave or in its vicinity. Under the influence of gravity the jet plunges down into the water generating a splash-up phenomenon and important turbulence generation (see for example Bonmarin¹). Generation of bubbles and spray is observed. Numerical experiments describing the evolution of breaking waves up to the time of impact of the jet have been developed successfully by numerous investigators using methods based on potential flows. Among the main contributions are the works of Longuet-Higgins and Cokelet,² Vinje and Brevig,³ Baker *et al.*,⁴ and New *et al.*⁵ This list is not exhaustive (see for more detailed reviews Peregrine,⁶ and Banner and Peregrine⁷). The process of the initiation of spilling breakers is less well understood. Two main mechanisms have been proposed. Computations of overturning waves by New *et al.*⁵ demonstrated that there is no essential difference between spilling and plunging breakers: the only difference is scale of the jet at the wave crest. This led these authors to suggest that spilling breakers might be produced by a small plunging event at the wave crest. More recently, Longuet-Higgins and Cleaver⁸ pointed out that a “crest instability” may represent the initial stage of the spilling breaker which has been found in laboratory by Duncan *et al.*⁹ This instability causes a bulge to form ahead the crest with capillary waves just below the “toe”.

There is little numerical simulation of this problem going beyond the time of impact of the plunging jet. In Monaghan *et al.*,¹⁰ the smoothed particle hydrodynamics method (SPH) was used to simulate a splash-up. However the spatial resolution of the method seems insufficient to resolve the small scale viscous and capillary effects. The aim of the present work is to attempt a preliminary numerical solution of the Navier–Stokes equations of this problem, on grids sufficiently fine so that viscous and capillary effects could be retained. We wish to simulate the two-phase flow of bubbles and droplets following splash-up as well as vortex-like motions. To this effect we have used a robust numerical technique, based on the volume of fluid method^{11–16} that allows us to use rather large grids and to follow large interface deformations and topology changes.

We consider viscous incompressible flow with a constant surface tension σ at the liquid-

gas interface. The governing equations for the velocity vector $\mathbf{u} = (u, v)$ and pressure p in the bulk of each phase (liquid and gas) are the classical Navier-Stokes equations supplemented by the condition of incompressibility:

$$\rho(\partial_t \mathbf{u} + \mathbf{u} \cdot \nabla \mathbf{u}) = -\nabla p + \nabla \cdot (\mu \mathbf{S}) + \rho \mathbf{g} + \sigma \kappa \delta_S \mathbf{n}, \quad (1)$$

$$\nabla \cdot \mathbf{u} = 0. \quad (2)$$

Here ρ is the density, μ is the dynamic viscosity, \mathbf{S} is the rate of strain tensor, whose components are $S_{ij} = \partial u_i / \partial x_j + \partial u_j / \partial x_i$, κ is the curvature, and \mathbf{n} is the a normal to the interface. δ_S is a delta function that is zero everywhere except at the interface. $\mathbf{g} = (0, -g)$ is the acceleration due to gravity. The location of the two fluids is specified with the help of a volume fraction function C , with $C = 1$ inside one fluid (liquid for example) and $C = 0$ in the other. An interface is to be constructed only if the fraction C is between 0 and 1. This is made by a volume of fluid type numerical technique, which is now well documented.^{11–16} This method allows us to follow interfaces beyond the point of reconnection, and is relatively simple and robust.

To simulate the wave kinematics and dynamics in infinite depth, we assume the motion to be two-dimensional and spatially periodic. The corresponding computational domain is a square cavity of length equal to the wavelength, λ , with periodic boundary condition in the direction of wave propagation and free-slip condition along the others. The reference length and time are chosen as λ and $(\lambda/g)^{1/2}$, respectively. As a result, four dimensionless parameters appear in the governing equations. They are the Reynolds number, $Re = \rho_L g^{1/2} \lambda^{3/2} / \mu_L$, the ratio of density, ρ_G / ρ_L , the ratio of viscosity, μ_G / μ_L and the Bond number, $B = \rho_L g \lambda^2 / \sigma$, where the subscripts L and G denote respectively the liquid and gas phases. Equations (1) in dimensionless form then read

$$\partial_t \mathbf{u} = -\mathbf{u} \cdot \nabla \mathbf{u} + \frac{1}{\rho} \left[-\nabla p + \frac{1}{Re} \nabla \cdot (\mu \mathbf{S}) + \frac{1}{B} \kappa \delta_S \mathbf{n} \right] + \mathbf{g}_u, \quad (3)$$

where $\mathbf{g}_u = (0, -1)$ represents a unit gravitational force. The dimensionless density ρ and viscosity μ in (3) are expressed in each cell, in the term of the volume fraction C as follows:

$$\rho = C + (1 - C) \rho_G / \rho_L; \quad \mu = C + (1 - C) \mu_G / \mu_L. \quad (4)$$

Instead of calculating the curvature of the interface, the (dimensionless) capillary force, $\kappa \delta_S \mathbf{n} / B$, is represented as the divergence of the capillary pressure tensor \mathbf{T} which is defined as $(\mathbf{I} - \mathbf{n} \otimes \mathbf{n}) \delta_S / B$, where \mathbf{I} is the unit tensor δ_{ij} . In this way, the capillary force is taken into account as a stress tensor which is computed from the gradient of the volume fraction C . Briefly, the Navier-Stokes equations (3) are solved using finite differences on a staggered (MAC) Eulerian grid and split-explicit time differencing scheme, while incompressibility (2) is enforced using an iterative multigrid Poisson solver. For full details of the method, readers are referred to Lafaurie *et al.*¹⁵ and Li,¹⁶ in which various tests of accuracy and validity are also given.

Previous numerical studies demonstrated that the details of wave breaking are very sensitive to initial conditions. Usually, two kinds of initial conditions have been used to generate wave breaking, one is the Stokes wave with a pressure forcing at the surface,^{2,4} another corresponds to an unsteady wave with a large enough amplitude.³⁻⁵ We present here the results for waves developing from the initial condition that corresponds to a Stokes wave in infinite depth calculated at the third order of wave amplitude a . Let x and y denote respectively the horizontal and vertical coordinates, and the origin be taken in the center of the cavity, then using the present scaling, the wave profile, η , of slope $\epsilon (= 2\pi a / \lambda)$ is as follows

$$\eta = \frac{1}{2\pi} \left[\left(\epsilon + \frac{1}{8} \epsilon^3 \right) \cos(2\pi x) + \frac{1}{2} \epsilon^2 \cos(4\pi x) + \frac{3}{8} \epsilon^3 \cos(6\pi x) \right]. \quad (5)$$

The numerical results of $Re = 2 \times 10^4$, $\rho_G / \rho_L = 10^{-2}$, $\mu_G / \mu_L = 0.15$ and $B = 10^4$ are presented in figures 1-3. The initial wave slope ϵ is set to be 0.55. Since it is not a steadily travelling wave and is steeper than any irrotational steady wave, such initial conditions evolve to breaking as shown below. Computation was done on a 256×256 uniform mesh with a constant time step of 10^{-4} .

Figure 1 shows a time evolution of liquid-gas interface and vorticity field up to time $t = 6$ (we recall that the present length and time scales were chosen such that a linear cosine

wave has a period of $(2\pi)^{1/2}$. (Complete movie stored as MPEG is available on the LMM WWW server (<http://www.lmm.jussieu.fr/Animations.html>). The initial wave given by (5) has its crest at $x = 0$ and progresses from left to right. At $t = 0$, the velocity field in the liquid part is obtained from the velocity potential at the third order (without surface tension, i.e. $B \rightarrow \infty$), while the gas is at rest, and then motion is generated in the bulk of the gas phase through dynamical coupling with liquid at the interface. As a periodic boundary condition is imposed in the direction of wave propagation, the fluid moving out of the domain on the right will rejoin it on the left. As can be seen, the wave breaks in the form of plunging. To distinguish the two phases, a color jump is used with green representing the liquid phase and grey the gas phase. However, in each phase, the values of vorticity are represented by different color levels; the maximum vorticity is shown by red and the minimum by blue. As shown in Fig.1(a), during the pre-breaking stage, the wave profile, particularly near the crest, becomes more and more asymmetric. The wave breaks at the time where the whole front face of the crest steepens and becomes vertical, and then a jet of liquid is projected forward into a characteristic overturning motion (Fig.1(b)). The vorticity in the liquid phase is mainly located in the vicinity of the tip of the jet where the curvature of the interface is important. Under the influence of gravity, the jet plunges down into the surface below, entraining a volume of gas (Fig.1(c)). The main effect of the impact of the jet is the generation of vortical motions under liquid and the formation of splash-up as shown in Fig.1(d). Strong vorticity is also generated at the crest of the secondary jet due to the splash-up. As pushed forward by the plunging jet, the second jet is growing in size (Fig.1(e)) and plunging (Fig.1(f)), generating second splash-up (Fig.1(g)). Third and fourth splash-ups are observed at $t = 3.48$ and $t = 5.12$, respectively. As shown in Fig.1(h), the wave loses most of its potential energy at $t = 6$, and splashing no longer occurs.

In order to gain further insight into the vorticity arising from the wave breaking, a close-up view of the active region in Fig.1(d), where the first splash-up is formed by plunging jet, is shown in figure 2. The velocity distribution of Fig.2(a) shows that the flow near the plunging

point displays a structure composed of two large vortices, one revolving clockwise (beneath the jet) and the other anticlockwise (in gas). The present mode of splash-up corresponds to one of modes described by Peregrine⁶ (see his Fig.4(b)): i.e. the jet penetrates the surface, and then, because of its forward motion and downward momentum, it acts like a solid surface and “pushes up” a jet of previously undisturbed flow, causing the splash-up. The vorticity distribution in this region is shown in Fig.2(b). The positive vorticity levels (solid line) are mainly concentrated in the regions where the first splash-up was formed, and at the crest of the second jet, while the negative vorticities (dashed line) are mainly located in the vicinity of entrapped gas. The change of direction in velocity and of sign in vorticity near the plunging point indicates that there exists a strong shear layer there.

Our numerical results of successive splash-up cycles and vortex-like motions agree qualitatively with the laboratory observations of Bonmarin.¹ However, the resolution (256×256) appears to be not fine enough; some of fragments of the liquid, as displayed in figures 1-2, does exist, which are due to the discretisation rather than physical effects. Simulations of higher resolution on grids of 512×512 and 1024×1024 are in progress; more detailed results will be reported in the near future.

Let E_k , E_g and E_σ denote respectively the kinetic energy, the gravitational potential energy and the capillary energy, calculated in the liquid part ($C \neq 0$) over one wavelength:

$$E_k = \frac{1}{2} \int \int_{C \neq 0} \rho \mathbf{u}^2 dx dy; E_g = \int \int_{C \neq 0} \rho y dx dy; E_\sigma = \frac{1}{B} (\Gamma - 1), \quad (6)$$

where Γ is the total arclength of liquid-gas interface. The total (mechanical) energy, E , is then obtained by summing these three parts.

The time evolutions of normalized values (by its initial value) of E , E_k and E_g , are plotted in figure 3. The initial values of the energies are respectively $E_k = 2.66 \times 10^{-3}$, $E_g = 2.23 \times 10^{-3}$ and $E_\sigma = 1.13 \times 10^{-5}$. This figure displays distinctly different regimes of the energy variation during the wave breaking process. Before the formation of the jet, the kinetic and gravitational potential energies decrease smoothly. After the jet formation ($t > t_1$) and under the influence of gravity, the jet plunges down, E_k increases up to the

time of impact of the jet onto the forward surface. The curves of E_k and E_g exhibit some small oscillations due to the formation of successive splash-up cycles generated by the first falling jet. Energy is dissipated by viscosity, therefore the total energy E decreases with the time. Its evolution, however, is not a linear function of the time. During the wave evolution, the slope of the total energy curve E , up to about $t = 4$, becomes steeper after the first 2 splash-ups, corresponding to a faster energy loss. It can be seen that nearly 70% of the total energy of the wave is lost after about three periods.

In summary, an initially steep short gravity wave with surface tension undergoing breaking have been simulated numerically; results show good resemblance to the laboratory observations of breaking water wave motions including overturning, plunging process, air entrainment, and successive splash-up cycles. The generation of vorticity both in the liquid and gas by the breaking process has also been shown. Energy dissipation due to viscosity has been found important during breaking process, particularly at the time of splash-up. We are currently working on a faster version of the code in order to simulate longer wavelengths. The ability of the code to simulate the dynamics of the gas phase also offers the perspective of simulating breaking waves in presence of wind.

ACKNOWLEDGMENTS

The authors wish to thank Prof. D.H. Peregrine for his helpful comments and suggesting improvements to the original manuscript, and Dr. P. Bonmarin for discussions. The computations were done on the SGI Power Challenge at IRPHE and in part on the SP2 of the CNUSC (Centre National Universitaire du Sud de Calcul). The support from DRET (Direction des Recherches, Etudes et Techniques) is gratefully acknowledged.

REFERENCES

- [1] P. Bonmarin, “Geometric properties of deep-water breaking waves,” *J. Fluid Mech.* **209**, 405 (1989).
- [2] M. S. Longuet-Higgins and E. D. Cokelet, “The deformation of steep surface waves on water. I. A numerical method for computation,” *Proc. R. Soc. London Ser. A* **358**, 1 (1976).
- [3] T. Vinje and P. Brevig, “Numerical simulation of breaking waves,” *Adv. Water Resources* **4**, 77 (1981).
- [4] G. R. Baker, D. I. Meiron and S. A. Orszag, “Generalized vortex methods for free-surface flow problems,” *J. Fluid Mech.* **123**, 477 (1982).
- [5] A. L. New, P. McIver and D. H. Peregrine, “Computations of overturning waves,” *J. Fluid Mech.* **150**, 233 (1985).
- [6] D. H. Peregrine, “Breaking waves on beaches,” *Annu. Rev. Fluid Mech.* **15**, 149 (1983).
- [7] M. L. Banner and D. H. Peregrine, “Wave breaking in deep water,” *Annu. Rev. Fluid Mech.* **25**, 373 (1993).
- [8] M. S. Longuet-Higgins and R. P. Cleaver, “Crest instabilities of gravity waves. I. The inner solution,” *J. Fluid Mech.* **258**, 115 (1994).
- [9] J. H. Duncan, V. Philomin, M. Behres and J. Kimmel, “The formation of spilling breaking water waves,” *Phys. Fluids* **6**, 2558 (1994).
- [10] J. J. Monaghan, P. J. Bicknell and R. J. Humble, “Volcanos, tsunamis and the demise of the minoans,” *Physica D* **77**, 217 (1994).
- [11] D. L. Youngs, “Time dependent multimaterial flow with large fluid distortion,” In *Numerical methods for fluid dynamics*, edited by K. M. Morton and M. J. Baines (Academic, New York, 1982) p. 27.

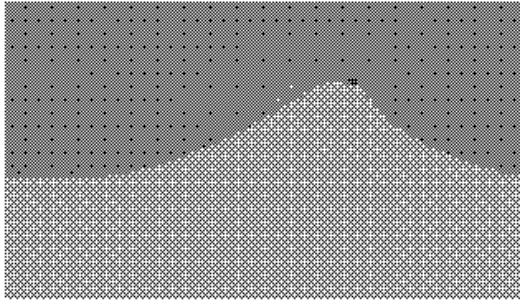
- [12] J. M. Hyman, “Numerical methods for tracking interfaces,” *Physica D* **12**, 396 (1984).
- [13] E. G. Puckett and J. S. Saltzman, “A 3d adaptive mesh refinement algorithm for interfacial gas dynamics,” *Physica D* **60**, 84 (1992).
- [14] N. Ashgriz and J. Y. Poo, “FLAIR: Flux line-segment model for advection and interface reconstruction,” *J. Compt. Phys.* **93**, 449 (1991).
- [15] B. Lefaurie, C. Nardone, R. Scardovelli, S. Zaleski and G. Zanetti, “Modelling merging and fragmentation in multiphase flows with SURFER,” *J. Compt. Phys.* **113**, 134 (1994).
- [16] J. Li, “Calcul d’interface affine par morceaux (piecewise linear interface calculation),” *C. R. Acad. Sci. Paris, série IIb* **320**, 391 (1995).

FIGURES

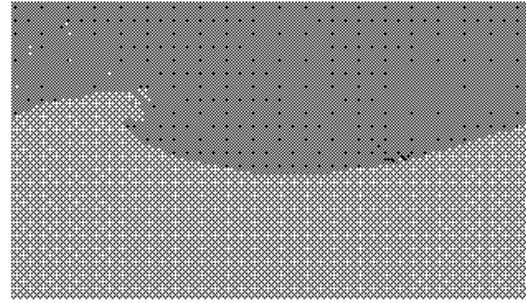
FIG. 1. Snapshots of instantaneous liquid-gas interface and vorticity field of a plunging breaker. Displayed region is $-0.5 \leq x \leq 0.5$ (corresponding to one wavelength) and $-0.3 \leq y \leq 0.3$. Physical parameters and initial conditions are given in the text. A color jump is used to simultaneously distinguish the two phases and represent vorticity: the liquid phase is mostly green and the gas phase grey. In both phases, high positive vorticity is red and very negative vorticity is blue.

FIG. 2. Close-up view of the active region of figure 1(d). The liquid-gas interface is represented by bold line. (a) Velocity field. The velocity vectors are plotted in every two computational cells. Maximum velocity is 0.96 (note that the velocity scale is $(g\lambda)^{1/2}$). (b) Contours of constant positive (solid line) and negative (dashed line) vorticity. Minimum and incremental levels of vorticity are -8.91 and 2.22 .

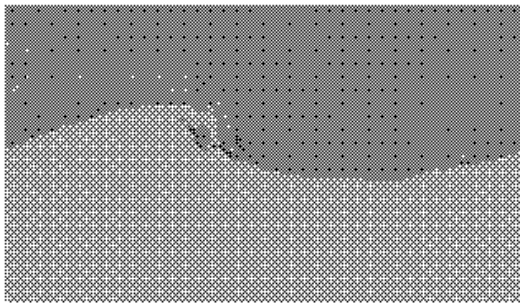
FIG. 3. The total energy ($E = E_k + E_g + E_\sigma$) (solid line), the kinetic energy (E_k) (dashed line) and the gravitational potential energy (E_g) (dashdot line), calculated in the liquid phase over one wavelength, as a function of the time t . Each energy is normalized by its initial value. Marked times correspond to respectively the formation of jet ($t_1 = 0.72$), the impact of plunging jet onto the forward surface and the generation of the first splash-up ($t_2 = 1.56$), the formation of the second splash-up ($t_3 = 2.84$), the formation of third splash-up ($t_4 = 3.48$) and the formation of fourth splash-up ($t_5 = 5.12$). The total energy E decreases due to viscosity. Nearly 70% of the wave energy is lost after about three periods.



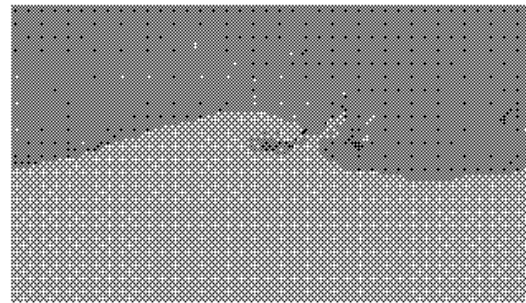
(a) $t = 0.24$



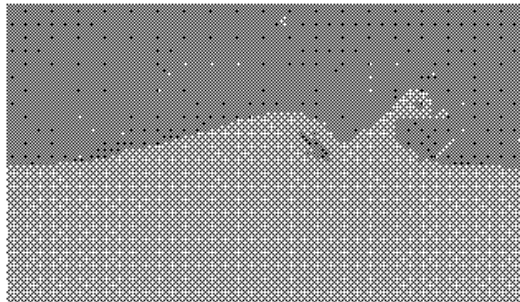
(b) $t = 1.28$



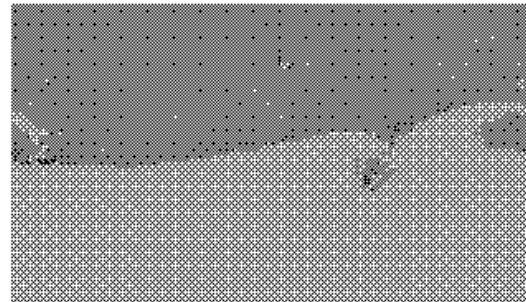
(c) $t = 1.56$



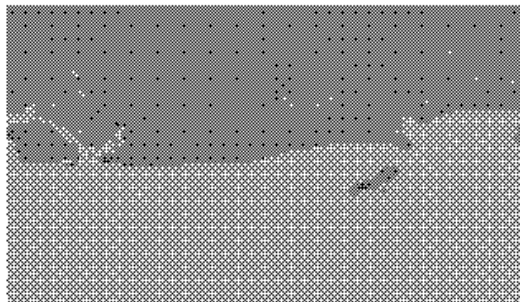
(d) $t = 1.92$



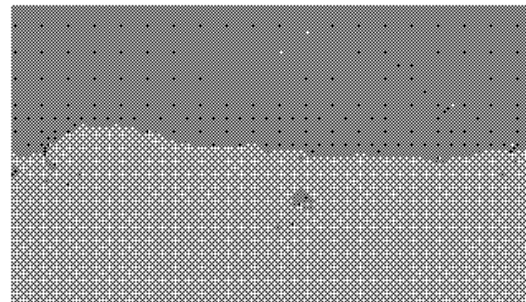
(e) $t = 2.28$



(f) $t = 2.72$



(g) $t = 2.92$



(h) $t = 6.0$

